Dynamics of Citrate Coordination on Gold Nanoparticles Under Low Specific Power Laser-Induced Heating

Danilo Oliveira de Souza, Jean-Sébastien Girardon, David J Hoffmann, Elise Berrier

Dynamics of Citrate Coordination on Gold Nanoparticles Under Low Specific Power Laser-Induced Heating

Danilo Oliveira de Souza, Jean-Sébastien Girardon, David J. Hoffmann and Elise Berrier

[a] Dr. D. Oliveira de Souza : ELETTRA Sincrotrone Trieste S.C.p.A., S.S. 14 Km 163.5, 34149 Basovizza, Trieste, Italy

E-mail: danilo.olsouza@gmail.com

[b] Dr. J.-S. Girardon, Dr. E. Berrier Université de Lille, CNRS, Centrale Lille, ENSCL, Univ. Artois – UCCS, Lille, France

[c] Dr. D. J. Hoffmann[+], Electrical Engineering Department, Federal University of Espírito Santo, (UFES), Vitória-ES, Brazil

[+] deceased author (2019)

Supporting information for this article i

D.O.I. 10.1002/cphc.202200744

Abstract

SERS evolution recorded over a drop-coated coffee-ring pattern of citrate-capped gold colloids was investigated as a function of time under low-specific laser power. Spectral changes caused by plasmon-induced reaction could not be detected, but a long-term transient original spectral profile showing additional lines was observed. We performed deep qualitative and quantitative SERS intensity variation analysis based on the complementary use of extreme deviation and cross-correlation statistics, which provided further insights on the behavior of citrate-capping layers of gold nanoparticles upon laser illumination. More precisely, the cross-correlation analysis made possible to follow the so-called individual events denoting particular resonance structures, in which groups of modes were assigned to an evolution of citrate coordination on gold surface driven by photo-activation. As a consequence, the detection limit was increased and new lines were related to the presence of a very low amount of dicarboxy-acetone (DCA), which was already present in the system.

Introduction

Nowadays, Surface Enhanced Raman Scattering (SERS) is well accepted as a powerful analytical technique, mainly due to the unique plasmonic properties of metal nanoparticles (NPs).[1] The basic components involved in this phenomenon are a molecule, a metal nanostructure and electromagnetic radiation, which introduces complexity in the interpretation of observed SERS spectra.[2-4] Particularly, the interaction of incident radiation with adsorbed molecules may lead to photodissociation, photoreactions or photo-desorption of those molecules deposed on the metallic surface of the nanostructure. Such effects are more pronounced, and of a special interest, when dealing with single molecule studies or ultra-sensitive SERS measurements. For instance, direct observation of heterogeneous photochemical reactions was reported based on the fluctuations in amino acid time-resolved SERS.[5] In that case, the authors were interested in the photochemical formation of amorphous carbon from aromatic precursors on Ag nanoparticles. Indeed, it is quite reasonable to suppose that depending on laser incidence and the arrangement of the nanoparticles (aggregations), the high electromagnetic fields induced on the hotspots could trigger photochemical processes. The classical example of this effect is the formation of graphitic or amorphous carbon by heating, giving rise to sp^2 stretching that appear as peaks around 1340 and 1580 cm^{-1} in Raman spectrum.[6-8]

Many studies have been dedicated to understanding some aspect of the photochemical reactions, seeking to correlate it with hot electrons that arise from plasmonic effect or some other thermal charge transfer mechanism,[9-11] but there is no final consensus.[12, 13] Essentially, hot electrons are produced upon resonant optical excitation of surface plasmons, becoming available to participate in photochemical reactions. The details on the generation of such hot electrons as well as the influence of molecular adsorbates and the representative processes are reviewed elsewhere.[12] Further, using molecular dynamics simulation, some works have inspected the light-induced heating of nanoparticles in molecular level and its propagation to the medium depending on the capping layer, which can cause molecular relaxation of the polymer coating,[14] and when increasing polymer density.[15] Other studies have performed numerical simulations to map the temperature distribution in nanoscale around nanoparticle networks[16-18] and the thermal processes of the light-to-heat conversion were reviewed theoretically and experimentally.[19]

Another aspect related to laser illumination of capped noble metal nanoparticles is the fluctuation SERS signal in time-dependent studies. The detailed origin of such behavior has been discussed in the last years and it is suggested that is arises from thermally activated diffusion of molecules bonded to the nanoparticle surface,[20] even though many physical and chemical processes take place at the same time adding complexities in its interpretation.[21] Particularly, those works related the presence of as-called “spurious SERS spectra” that were not related in principle to the studied analyte deposited on the metal

surface.[20, 22] It was observed that even low-energy thermal processes can lead to reversible ionization at SERS-active sites, thus not related with an eventual photodecomposition.[20]

Actually, thermal photochemistry reactions should not happen at low laser power, which it does not mean that other photoinduced effects are not present during a laser illumination, particularly if in resonance condition.[23-25] Fluctuations in the intensity of SER lines, wiggles and popping up of extra lines are not random and may raise upon laser illumination without trigging thermal-reactions, as already reported for silver nanoparticles.[26, 27] Fluctuations on the Raman bands were reported on carbon clusters deposited on rough metal substrates using weak laser power (5 mW/cm^2 at the sample).[8, 28] Of a special interest, it is noteworthy to say that the fluctuations occurred only in presence of oxygen, indicating a photooxidation process and CO molecule adsorption at the metal.[8] In this picture, even if great advances in understanding the interaction of capping layers and the nanoparticles have been done, it seems elusive to get further insights on the binding modes of citrate on the gold surface as well as the existence of possible photoreaction products of citrate at a single-particle level.

Here, we perform low-intensity laser power high resolution time-resolved SERS measurements in pre-localized surface plasmon resonance (LSPR) condition and we discuss intensity fluctuation in SERS spectrum in terms laser induced heating of nanoparticle in a non-destructive condition, *i. e*., without trigger photochemical reactions within nanoparticle's capping layer. We present a quantitative and qualitative investigation of the individual events occurring in time using a methodology we developed earlier and described elsewhere[29] to verify the influence of lighting on the capping layer of the nanoparticles as well as an eventual changing on the sensibility of SERS detection. In particular, we focus on the fluctuations on the COO^- and CC stretch vibrations detected, respectively, in the 1500–1620 cm^{-1} and 950–1050 cm^{-1} ranges. We correlate these features with the fluctuations of different bond modes of the citrate to the nanoparticles along laser illumination.

Experimental Methods

Gold nanoparticles were synthesized via classic citrate reduction (aka, Turkevich method) described elsewhere.30 Briefly, 12.5 mL of HAuCl4 (5.4 mmol L−1) was added to 213 mL of milli-Q water and stirred at 75 °C. The temperature was subsequently increased until the temperature reached 80 °C. 25.0 mL of sodium citrate (5.4 mmol L−1) was added, so that the value of the cit./Au molar ratio is 2.

SER spectra were recorded using a He−Ne laser for excitation (632.8 nm), and the power at the sample of 0.04 mW (5500W/cm2), adjusted using neutral density filters. The laser beam was focused on the contour line of the coffee-ring pattern (i. e., the pattern left by the puddle of the liquid solution after it evaporates) of the sample using a 100x microscope objective (NA 0.9). The Raman signal was collected in backscattering mode using the same objective through a confocal hole of 150 µm. The scattered light was

dispersed using a spectrometer equipped with a 600 mm-groove grating and analyses by a Peltier-cooled CCD (Horiba Labram HR). For a series of SERS spectra of 10 minutes, we have used an acquisition time of 20 seconds per scan, with a rest time between two consecutive spectra of 40 seconds. Measurements were performed on regions where isolated nanoparticles could be found, since large NP aggregation could imply in different LSPR spectrum and, thus prevent a pre-resonance condition. All spectra were normalized with regards to their overall area and a nonlinear baseline correction (BL) were applied.

Electrospray ionization-Mass spectrometry (ESI-MS) in positive-mode was performed before laser illumination, using the supernatant solution, which was diluted with methanol in a ratio of 1 mg/mL, then directly infused at a flow rate of 5 $\mu L.min^{-1}$ into the ESI source. The mass spectrometer (model 9.4 T Solarix; Bruker Daltonics, Bremen, Germany) was set to operate over a mass range of 200–2000m/z. The ESI source conditions were as follows: nebulizer gas pressure of 1.5 bar, capillary voltage of −3.6 kV, and transfer capillary temperature of 200 °C. Ions time accumulation was 0.060 s and the FT-ICR mass spectra were acquired by accumulating 16 scans of time-domain transient signals in 512k time-domain data sets. All mass spectra were externally calibrated using NaTFA (m/z 200–2000). A resolving power, $m/\Delta m_{FWHM} \cong 530\,000$, in which Δm_{FWHM} is the full peak width at a half-maximum peak height of $m/z \cong 400$ and a mass accuracy of <3 ppm, provided the unambiguous molecular formula assignments for singly charged molecular ions. Mass accuracy is determined from mass error, defined as $Error=((m/z_{measured}-m/z_{theoretical})/m/z_{theoretical})\times 10^6$. The mass spectra were acquired and processed using Data Analysis software (Bruker Daltonics).

Results

Raman spectra were collected at a coffee-ring pattern obtained from a cit-AuNP drop deposited over a microscope slide and let dried under ambient conditions at room temperature. Both the selected laser power and the acquisition time were deliberately kept very low to ensure that no non-reversible chemical change occur in the citrate layer. At 633 nm laser wavelength, the system is in pre-resonance condition regarding the plasmonic frequency of AuNPs. As a result, only limited sample heating is expected, although the Raman exaltation was highest.

The reference Raman spectrum of aqueous citrate is presented in Figure1 and a tentative assignment of its main features is presented in Table S1 (see supporting information). Of particular interest for our system is the study of the COO^- and CC stretches vibrations (respectively, around 1550 and 990 cm^{-1}) because they can tell us how the citrate is coordinated to the gold nanoparticles, as discussed by Grys *et al*.[31] In the case of the CC stretch region, the conventional Raman spectrum of aqueous citrate shows Raman lines at 940, 1052 and 1082 cm^{-1} while only SERS lines were detected at 968, 1004 and 1025 cm^{-1} for cit:AuNP (Figure 1). Similarly, the stretches regions of COO^- mode present a blue shift with respect to ordinary acid citric. Dominant SERS modes are assigned to the bidentate coordination with the central

carboxylate (red) as well as bonds from terminal carboxylates (blue). The SER spectrum of the freshly prepared cit:AuNPs coffee-ring assemblies is in line with previous reports[32-35] and suggests that the citrate is chemisorbed to the gold via the carboxylic groups. Curiously, some SERS bands (particularly, 1004, 1120, 1247, 1270 and 1365 cm^{-1}) strongly indicate the presence of dicarboxyketone on the surface of AuNP (see Figure 1), which is not surprising, since this phenomenon was finely discussed before.[36] This find is further supported by our ESI-MS measurements (see below).

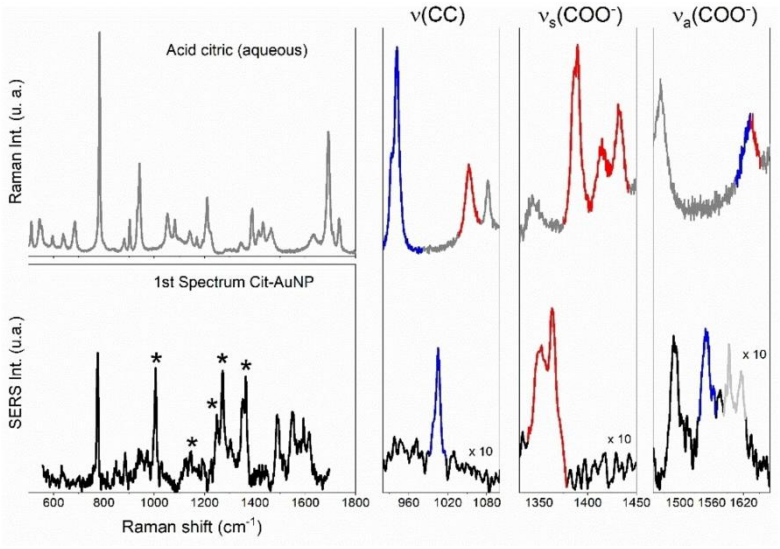

Figure 1: Citric acid Raman vs. citrate-capped Gold Nanoparticles SERS. Blue or red highlights on the spectra are related to coordination of a particular carboxylate position, respectively, terminal or central. Symbols (*) represent the bands that can be assigned to dicarboxyketone.

We have investigated the evolution with time of the SER signal by following the same approach as Smith *et al.*[29] for refining the probability and amplitude of the occurrence of particular spectral signatures observed transiently while repeating a large number of SERS acquisitions over time. To this end, we have collected one spectrum every minute during one hour, the acquisition time for each spectrum is of 20 seconds while the sample is left in the dark (laser off) for 40 seconds.

Time-Resolved SERS

The comparison of the first (*t*=60 s) and last (*t*=3600 s) SER spectra presented in Figure S1' confirms that no degradation of the capping layer has occurred during the whole analysis. Indeed, no laser- (or heat-) induced modification that would lead to significant broadening of Raman modes and formation of carbonaceous species with typical D and G-like carbon lines was observed.[37] Usually, when destructive processes over time are accompanied by unambiguously quality deterioration, such as decreasing of peak intensities and peak broadening,[38] which would make the summed (or averaged) spectrum like the typical carbon broad-band features.[8] Instead, we observe that the relative intensity of some vibrational modes was drastically modified during the experiment as well as the rising of new lines without significant quality deterioration.

In order to re-build the chronicle of such evolution, we propose here a qualitative investigation of the time-lapsed SER features over the whole set of collected spectra. To this end, time-dependent evolution of SERS spectra is showed in Figure 2.

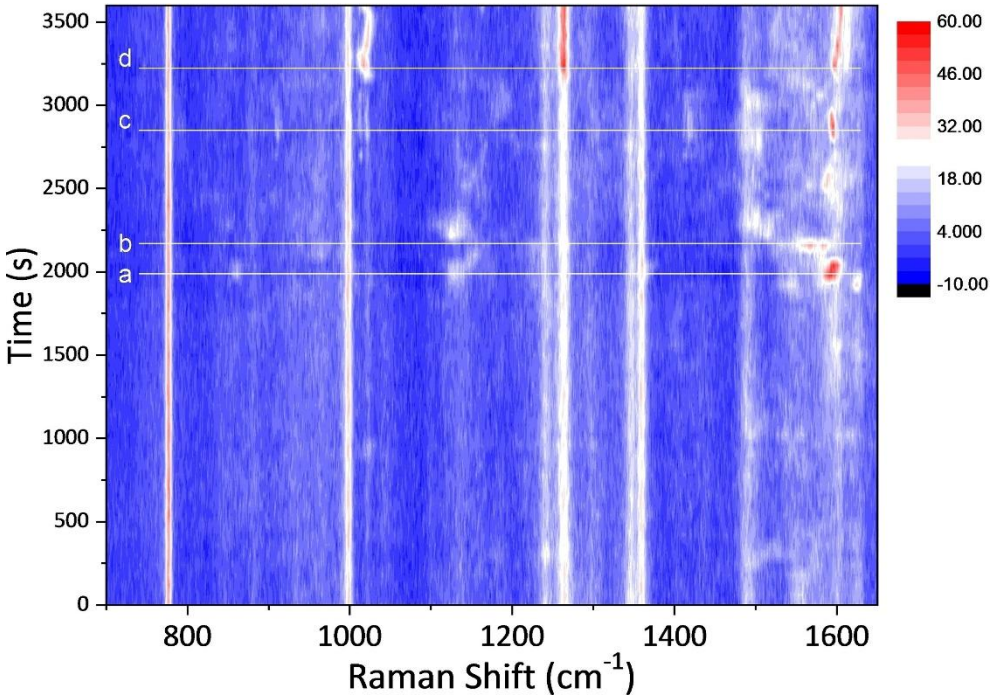

Figure 2: Time-resolved spectral evolution of citrate capping gold nanoparticles illuminated with a laser power of 0.04 mW. Each row represents one color-coded spectrum with time running from bottom to up. Solid white lines mark particular events (see text).

All spectra were normalized with respect to their overall area after a baseline correction. By doing so, we remove the continuous background emission from the SER spectra as well as we assure that each individual measurement and peak is independent of the dose received from laser. Main SERS bands present during the whole process are observed at 775, 1004, 1270, 1352 and ~1600 cm^{-1}. Interestingly, no remarkable changes are detected before 1920 seconds, which has been also observed for other sets of experiments, i. e., a measure made with the same parameters, on the same sample, but in a different region (Figure S1''), suggesting that the generation of such fluctuations is an activated process. In the second part of the experiment (from 1900 s), we clearly point individual events on the spectral evolution. Indeed, not only variations in the relative intensity of lines are detected, but also frequency shifts and/or transient occurrence of new lines. The instant *a* on the figure marks the first remarkable event on our experiment (at *t*=1980 s), an important increase in the intensity of the broad line centered at 1595 cm^{-1}, which hold its value during 2 consecutive spectra (or 120 s, in total). As soon as the intensity fluctuation ends and the intensity backs down to an ordinary value, we observe a second (shorter) one, now at 1565 cm^{-1} followed by simultaneous blinks at 1500 and 1130 cm^{-1} (mark *b*, in Figure 2, *t*=1980 s). Mark *c* (*t*=2880 s) points to another blink in the same (but sharper, this time) region centered at 1595 cm^{-1}, whereas the mark *d* (*t*=3240 s) is characterized by multiple concomitant events, namely, the rise of the

Raman line at 1025 cm^{-1} followed by a slight wiggling, the increased intensity of the 1270 cm^{-1} line and the shift to higher position of the peak centered at 1595 cm^{-1}.

In order to quantify properly an eventual correlation between lines and fully portrait the species present, we provide in the following a 2D correlation picture showing the covariance map of the dataset.

Analysis of Covariance Between SER Lines

The adopted approach[39] consists in compare quantitatively the variation in spectral intensity over the time of the experiment (*t*) considering two different wavenumbers, said v_n and v_m and calculating their covariance value, X(v_n, v_m):

$$X(v_n, v_m) = < I(v_n, t) \cdot I(v_m, t) > \qquad (1)$$

and represents the coincidental trends (or dissimilarities) of intensities from two different wavenumbers as *t* is scanned. The symbol <…> denotes for a cross-correlation function. The so-called *synchronous* 2D correlation map, in a set of discrete dynamic spectra measured at equally *k* spaced points, can be calculated in a way very similar to the statistical covariance of the spectral intensity with *k −1* degree of freedom, as follows:

(2)
$$\Phi(v_n,\ v_m) = \frac{1}{k-1}\sum_{j=1}^{k} I_j(v_n) \cdot I_j(v_m)$$

Where $I(v, t_j)$ is the spectrum at time equals to t_j subtracted from a reference spectrum, usually the averaged one. Our synchronous 2D correlation map is shown in Figure 3. Typical from these constructions, one observes a symmetry with respect to a diagonal line corresponding to coordinates v_n=v_m, with correlation peaks appearing at both diagonal and off-diagonal positions. Negative correlation values give purple traces whereas positive values are gradually represented by light blue to red regions (see color scale on the right). Any region of a spectrum which changes intensity to a great extent under a given perturbation will show strong autopeaks (the diagonal peaks), while those remaining near constants develop little or no autopeaks.

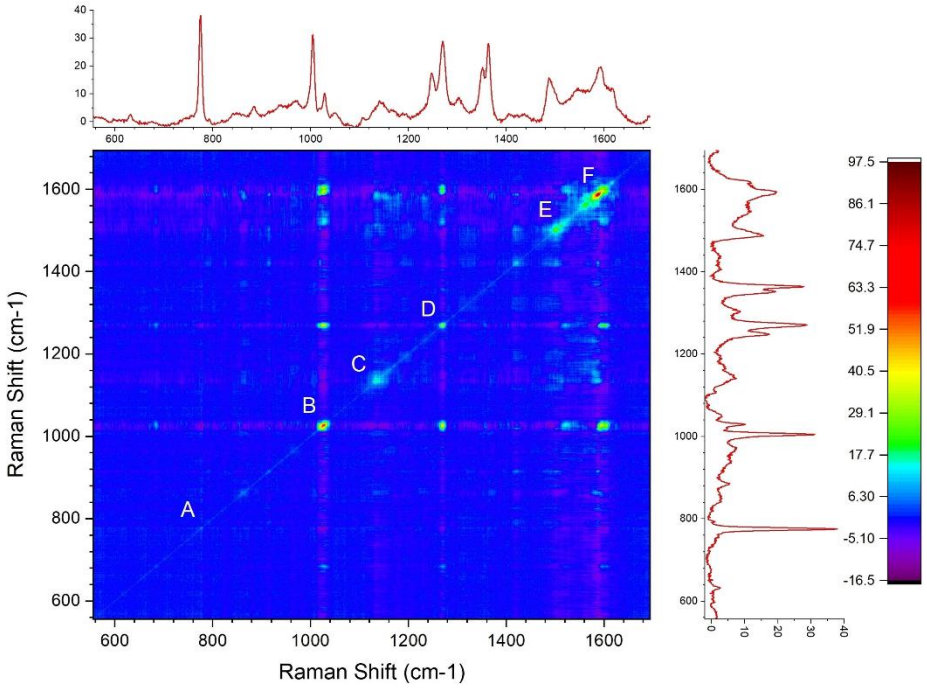

Figure 3: Synchronous 2D Raman plot. Reference spectrum at the top and right of the contour map is the average spectrum. Capital letters highlight some of the main autopeaks on the analysis. A to F corresponds respectively to the peaks/regions centered around 775, 1025, 1130, 1270, 1500 and 1587 cm^{-1}.

For instance, Figure 3 tells us that the peak centered at 775 cm−1 (the A spot) has a dull autopeak as consequence of its stable intensity during the whole experiment. Equally, those evident lines seen in Figure 2 (1004, 1247, 1348, 1362 and 1485 cm−1) present no autopeaks, except 1270 cm−1 (which corresponds to autopeak D). The strongest autopeaks are marked with capital letters, from B to F. Peak B, centered at 1025 cm−1 has strong positive correlation with peaks D (1270 cm−1) and F (~1587 cm−1), but just weak with respect to E autopeak (~1500 cm−1). On the other hand, feature C (1130 cm−1) seems to have no clear positive correlation with any other spectral feature. Actually, there are other spots on the 2D plot that behave on the same way, however they can be barely seen because they do not present strong autopeaks. Feature A is one of them, together with weak spots at 680, 863, 915, 1190 and 1420 cm−1. It is easily verifiable that autopeak A comes from a SERS peak with stable intensity. Besides it, for the other bands the reason is they are just flash signals along the experiment and may be considered as individual events (see Figure S2', where these events could be highlighted after perform a subtraction of each spectrum by the first component taken from Principal Component Analysis).

So far, it seems the system evolves to a final stage in which a further contribution appears after isolate and transient events. On next, we go deeper on the analysis to isolate the concomitant events, then give them a proper hypothesis.

Individual Events Analysis

In order to isolate these individual events, we performed temporal profile analysis of the intensity of selected lines (Figure 4A). The criterion to be considered as an individual event is described as following: the averaged intensity (Avg) and the standard deviation (σ) were evaluated. Individual events were defined as the events showing at least an intensity value as high as the threshold of Avg+3σ. Such flash events on the spectra, can be checked also by means of the excess Kurtosis coefficient defined for each Raman shift over time as:

(3)

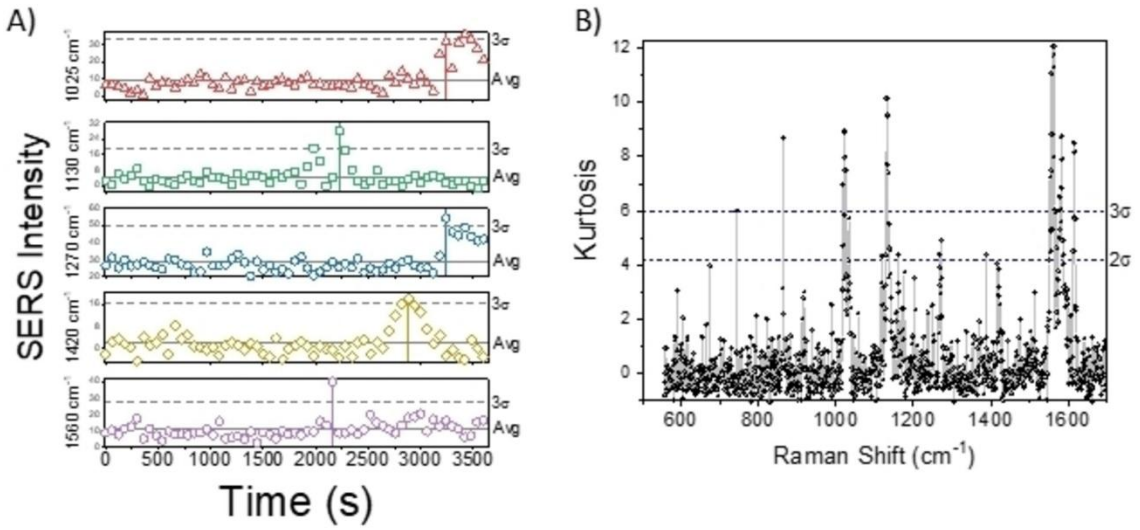

Figure 4: A) SERS intensities of selected bands as function of time highlighting the flash behavior. Average values for each series together with the defined threshold (see text) are also plotted for reference; vertical bars are guide for the eyes, showing the point of maximum. B) Kurtosis values as a function of wavenumber for the whole data set.

where μ^4 is the fourth moment about the mean and σ is the standard deviation. The Kurtosis plot has the ability to show us particular lines on a SER spectrum that contain an outlier (a flash event, in our case) either due to a high degree of abnormality of the intensity or due to a significant contribution of a new signal.

Figure 4B shows the Kurtosis coefficients as a function of the Raman shift for our experiment. It reveals that individual events happen in a wide range of the spectrum along the laser exposure. Considering the threshold of 3σ (three times the standard deviation), we have outliers in our series at 863, 1016, 1025, 1132 cm^{-1} and the wide region ranging from 1550 to 1620 cm^{-1}. Some of the bands coincide with those found on 2D plot of Figure 3. Even though the band at 1420 cm^{-1} is absent in Kurtosis plot, its intensity profile vs. time (Figure 4A) does suggest an individual event (also supported by Figure S2'). It seems that the smooth increasing of its intensity along the time (Figure 4A) was enough to put down its Kurtosis coefficient. Further, one observes that 1016 cm^{-1} and 1025 cm^{-1} points at Kurtosis plot correspond

actually to the same feature at the time evolution of Figure 1 that arises at *t*=3240 s and slightly wiggle until the end of the experiment.

Since the time lapse of one of our SER spectra is far bigger (by several orders of magnitude) than the time characteristic lifetime of intermediate chemical species, we interpret these features in the context of single molecule detection. A selection of SER spectra corresponding to these individual events is presented in Figure S3' and Figure S4' shows the intensity along the time. All new peaks or peak blinks emerge from 1980 seconds on, which is our first mark point on the time-resolved plot on Figure 2 (the horizontal line with label *a*). It seems that some of the events are undoubtably linked and we will discuss them based on recent studies related to the citrate coordination and bridging modes to nanoparticles.[25, 31]

In the beginning, vibration bands such as 632, 848, 940 and 1591 cm^{-1} suggest that citrate molecules attached to the gold nanoparticles has a coordination mode in which at least one or two carboxylates are non-bound to the gold (see Table S1). This coordination is quite stable up to *t*=1920 s. Then, our system starts to suffer modifications. Based DFT calculations performed by Grys et al.,[31] it was found seven possible coordination modes that citrate can be fitted when trapped between two gold nanoparticles (some of these modes are drawn on SI, see Figure S6'). Accordingly, we can associate those individual events from Figure S3' and Kurtosis analysis to one or two of the modes found on calculations. For instance, the vibration at 863 cm^{-1} may be associated to the modes c_2-t_2 or c_2-t_2t_2. The band at 915 cm^{-1} may be due to the c_2t_2-t_2 mode as also the c_2 mode. 1138 cm^{-1} vibration (and also 1132 cm^{-1}) can be linked to c_2-t_2 or t_2t_2 modes, while the ones at 1151 and 1171 cm^{-1} can be connected to the c_2-t_2 mode. The band at 1420 cm^{-1} is present at the c_2-t_2 mode as well as c_2 or t_2. Finally, 1560 cm^{-1} arises in c_2-t_2 mode or c_2. It is worth to note that among the calculated DFT modes, in three (c_2-t_2, c_2-t_2t_2, c_2t_2-t_2) we have central and terminal carboxylates bound in adjacent nanoparticles, spanning the citrate on the Au surface. The condition to such situation is to have low surface coverage to allow the span a small gap between the neighbor nanoparticles.[31]

Even though in literature Raman lines 680, 863, 1150, 1170, 1220 and 1540 cm^{-1} are reported as being due to CO, H_2O_2, O_2 or HO_2^- adsorption on gold surface,[40-46] our recorded spectra are out of range for a suitable analysis of these hypothesis. For instance, it is actually on the range 1800–2100 cm^{-1} one can accurately observe the CO contribution.[47] Thus, we cannot exclude this possibility, but we have no further evidence that these adsorption processes may occur undoubtedly in our experiment.

Particularly, the CC-stretches in combination with the asymmetric COO-stretches, found on the region from 1580–1620 cm^{-1} deserves a special attention because it is the zone where the citrate bridges to the gold nanoparticles. Thus, the vibrations there in are enough to differentiate these modes in a SER spectrum.[31] Thus, we performed accurate analysis of this region along the last instant of our experiment, since it is where the system passes by an intense variation as seen in Figure 2 and as suggested by the Kurtosis coefficients (Figure 4B). Figure 5 shows in more details the region of interest in the time range

t=2700–3600 s. The first abrupt change in intensity happens for the peak around 1590 cm^{-1} at t=2820 s. During the lapse of 3 scans, it remains at the same position for (blue curves), then disappear for 4 scans (grey curves) to then reappear blue-shifted and evolves slightly across high frequencies (green curves). This reappearance comes together with the arise of a new band around 1605 cm^{-1}. A similar trend concerning its centroid position is clearer when observing the plot of results for the peak fitting (Figure 5A, right panel; the color zones follow those from the left panel). Also, from the fit, one observes that the areas of the peaks tend to remain constant (with neither significant variation of the FWHM values), if we ignore (for obviously reasons) the brief time when the peak around 1590 cm^{-1} disappears (the grey area). Thus, one can say that there is an actual blue shift of the two main peaks in these regions (black and red dots). A similar analysis (Figure S5') is performed in the region from 980–1050 cm^{-1}, where it is observed the wiggle band (~1025 cm^{-1}) at the end of the experiment (from *t*=3180 s).

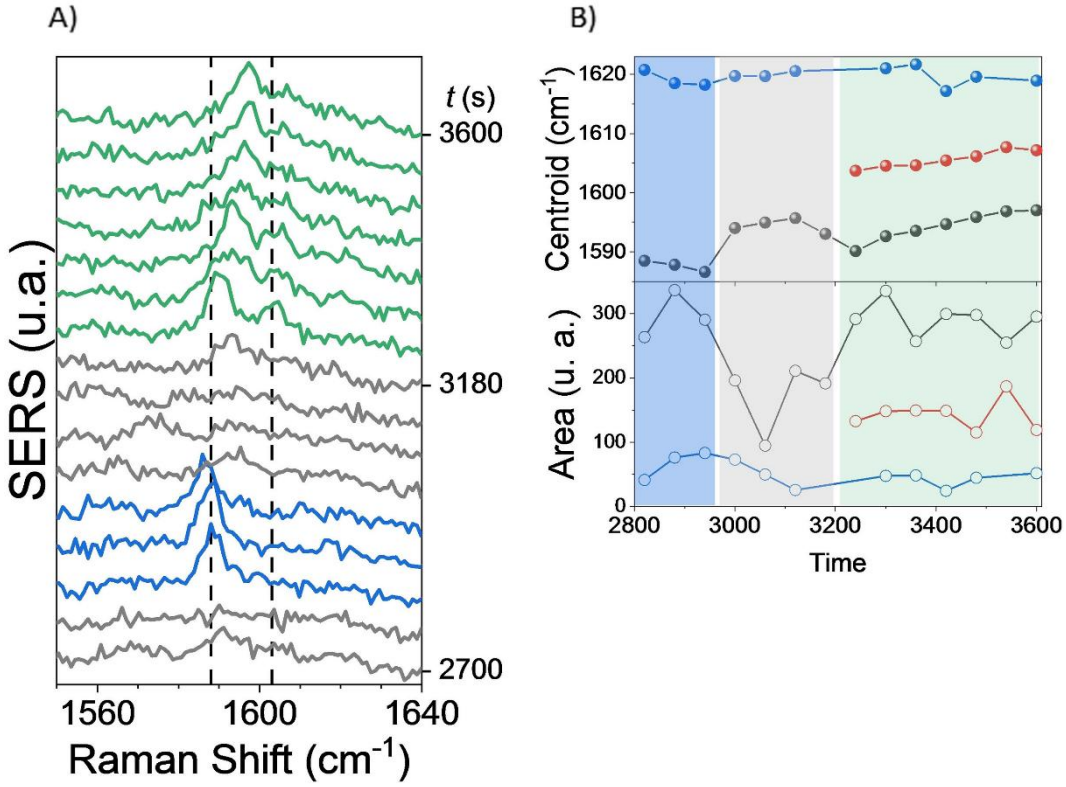

Figure 5: A) SER spectra from 2700 s up to 3600 s on the 1550–1640 cm^{-1}; the dashed lines are guide for the eyes. B) Centroid and Total Area evolution obtained after the fit of individual spectra.

Thus, individual events are suggested as being a transient step on the process of a new conformation of the capping citrate on hotspots of gold surface, while increasing in intensity and rising of new peaks are coincident with this new arrangement, as showed by the covariance correlation. Looking at the difference of the last and the first spectra in our dataset (Figure S1'), we realize that two new intense peaks appear at the end, which are attributed to the new coordination mode c2-t2 and to the dicarboxy acetone (DCA) (see Table S1 and S2), as confirmed by Mass Spectrometry (below). The further modifications of the spectra are attributed mainly to the reconfiguration of citrate (see Table S1).

Mass Spectrometry Analysis of cit-AuNP Solution

We carried out ESI-MS to check if before the experiment any byproduct of citrate reaction was produced during the synthesis. Figure 6 shows us the full scan ESI-MS in the range m/z=200–1100. The build-block of our system, aka citrate radical, has m/z=191 and it is out of our range of measurement. However, we can recognize a lot of structures that are closed linked to it, particularly bounded to a gold atom. Actually, ESI−MS is known to produce fragmentation (by collision dissociation) and to form dimers such as $[2\ M+H]^+$ or $[2\ M+Na]^+$ when analyte concentration is increased.[48-52]

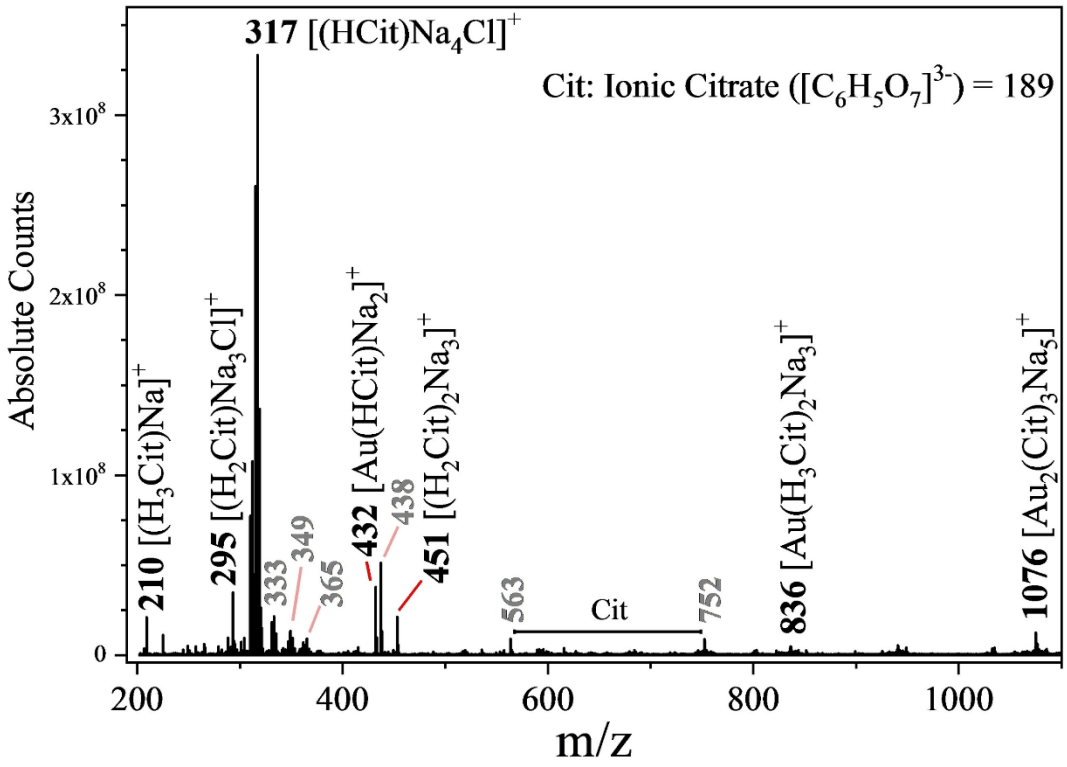

Figure 6: Full scan ESI mass spectrometry of citrate-AuNP recorded in positive ion mode. $(C_6H_5O_7)^{3-}$ is the molecular building block, named "Cit". m/z is the mass-over-charge ratio of the detected compounds.

We kept our attention to the molecular formulas containing the molecular building blocks of the measured ligand (for example, C_6 and O_7 and their multiples for citrate) with a matching isotope pattern ($^{12/13}C$ plus the corresponding heteroatoms of the calculated molecular formulae), but eventually we found also contributions from fragmented complexes, such as dicarboxy acetone (DCA), in very low concentration (as viewed by the relative peak height, named, 365 and 563) or almost insignificant. The fragments are assigned in grey in Figure 6 and the list of the possible candidates are written in Table S3. DCA is a well-known product from synthesis that may be present as capping AuNP or as a supernatant.[53]

It is worth to note that ESI-MS points to an excess of Na^+ ions attached to the citrate, which is a condition that favors shorter distance among the gold nanoparticles, enabling the appearance of the c_2-t_2t_2 SERS modes.[31] The temporal evolution experienced by our system suggests that citrate anions undergo

temperature-dependent conformational changes. Thus, we hypothesize that our system suffers a photo-induced coordination transformation from single citrate molecules bounded to gold atoms (c_2, t_2 vibrational modes) to single citrate molecules being coordinate by different Au atoms (c_2-t_2t_2, c_2-t_2 and c_2t_2-t_2). These changes could happen locally on the hotspots between two nanoparticles as a result of, for instance, the evaporation of the residual water eventually present on our sample during SERS experiment. Such evaporation caused by the heat transfer could allow the nanoparticles to relax and decrease the gap among them, stablishing a new local arrangement concerning citrate coordination. Further, this transformed disposition would induce the formation of additional hot spots (or increased SERS enhanced factors), making detection of previously present low-concentrated byproducts or fragments easier and more evident, particularly, DCA molecules. Indeed, a photoinduced system evolution leading to amplification of detection for similar systems has been already reported and discussed in literature.[31, 54]

Conclusions

We have shown that even under very low-power laser illumination, the citrate cap layer of gold nanoparticles synthesized by classic citrate reduction undergo a net transformation as seen by relative long-term time-resolved SERS experiments. We have demonstrated that it is possible to refine the citrate-gold bond modes by using the Kurtosis descriptor, the time-evolution of reaction product characteristic lines and the covariance values in a complementary manner. We have given a step forward in the using of such methodological method of analysis, not only applied to chemical reactions but now to local and subtle coordination changes that can lead to increased enhancement SERS amplification. Accordingly, our hypothesis is that laser induced a local surface reconfiguration without trigger any chemical reaction that changed the coordination between citrate and adjacent nanoparticles. Individual events could be due to a transient SERRS phenomenon allowed by the thermally activated formation of particular local resonant structures via charge-transfer processes. As consequence, besides the citrate capping the nanoparticles, we could increase the sensibility to extreme low concentrated fragments that were eventually present on the hotspots, such as dicarboxy acetone.

Supporting Information Summary

- Assignment of Raman and SER bands
- Tentative of assignment of SERS/Raman bands (Table S1)
- First and last spectra after 1 h irradiation (Figure S1')
- Evolution of SERS in a different spot of the sample (Figure S1'')
- SERS bands for Citrate byproducts (Table S2)
- Analysis of Individual Events
- Difference contour plot of SER spectra by PC 1 (Figure S2'

- SER spectra corresponding to the events of Figure S1 (Figure S3')
- Intensities in function of time of extra bands (Figure S4')
- Close analysis of the 1025 cm^{-1} band from t=3180 s (Figure S5')
- Mass Spectrometry cit-AuNP solution
- Tentative of assignment of ESI-MS lines (Table S3)
- Citrate Coordination Modes of Gold Nanoparticles
- Selected Coordination Modes as Calculated by DFT (Figure S6')
- Additional references cited within the Supporting Information.[55-58]

Acknowledgments

We are enormously thankful to the Prof. Dr. Jeremy J. Baumberg from The Cavendish Laboratory – Department of Physics of University of Cambridge, for gently share data of DFT simulations and SERS/Raman from citrate thermo-decomposition products. The authors thanks also Prof. Dr. Wanderson Romão, from Chemistry Department – Federal University of the Espirito Santo (UFES) for the ESI-MS measurements and the CNPq (Centro Nacional de Pesquisa Científica, Brazil) for financial support of David J. Hoffmann (*In memoriam*).

References

[1] M. Moskovits, Rev. Mod. Phys. 1985, 57, 783.

[2] R. Aroca, Surface-Enhanced Vibrational Spectroscopy, John Wiley and Sons, Chichester, 2007.

[3] R. Aroca, S. Rodriguez-Llorente, J. Mol. Struct. 1997, 408–409, 17–22.

[4] R. F. Aroca, R. A. Alvarez-Puebla, N. Pieczonka, S. Sanchez-Cortez, J. v. Garcia-Ramos, Adv. Colloid Interface Sci. 2005, 116, 45–61.

[5] E. J. Bjerneld, F. Svedberg, P. Johansson, M. Käll, J. Phys. Chem. A 2004, 108, 4187–4193.

[6] R. A. Álvarez-Puebla, J. Phys. Chem. Lett. 2012, 3, 857–866.

[7] A. Otto, J. Raman Spectrosc. 2002, 33, 593–598.

[8] A. Kudelski, B. Pettinger, Chem. Phys. Lett. 2000, 321, 356–362.

[9] M. A. Mahmoud, Phys. Chem. Chem. Phys. 2017, 19, 32016–32023.

[10] P. Selvakannan, R. Ramanathan, B. J. Plowman, Y. M. Sabri, H. K. Daima,

A. P. O'Mullane, V. Bansal, S. K. Bhargava, Phys. Chem. Chem. Phys. 2013, 15, 12920–12929.

[11] O. A. Yeshchenko, I. S. Bondarchuk, V. S. Gurin, I. M. Dmitruk, A. v. Kotko, Surf. Sci. 2013, 608, 275–281.

[12] Y. Zhang, S. He, W. Guo, Y. Hu, J. Huang, J. R. Mulcahy, W. D. Wei, Chem. Rev. 2018, 118, 2927–2954.

[13] E. L. Keller, R. R. Frontiera, ACS Nano 2018, 12, 5848–5855.

[14] J. Soussi, S. Volz, B. Palpant, Y. Chalopin, Appl. Phys. Lett. 2015, 106, 093113.

[15] S. Ju, B. Palpant, Y. Chalopin, J. Phys. Chem. C 2017, 121, 13474–13480.

[16] A. Sanchot, G. Baffou, R. Marty, A. Arbouet, R. Quidant, C. Girard, E. Dujardin, ACS Nano 2012, 6, 3434–3440.

[17] V. Yannopapas, J. Phys. Chem. C 2013, 117, 14183–14188.

[18] N. Zeng, A. B. Murphy, Nanotechnology 2009, 20, 375702.

[19] V. K. Pustovalov, RSC Adv. 2016, 6, 81266–81289.

[20] S. R. Emory, R. A. Jensen, T. Wenda, M. Han, S. Nie, Faraday Discuss. 2006, 132, 249–259.

[21] T. Itoh, Y. S. Yamamoto, Analyst 2016, 141, 5000–5009.

[22] P. C. Andersen, M. L. Jacobson, K. L. Rowlen, J. Phys. Chem. B 2004, 108, 2148–2153.

[23] P. G. Etchegoin, P. D. Lacharmoise, E. C. le Ru, Anal. Chem. 2009, 81, 682–688.

[24] K. Chaudhari, T. Ahuja, V. Murugesan, V. Subramanian, M. A. Ganayee, T. Thundat, T. Pradeep, Nanoscale 2018, 11, 321–330.

[25] T. Ahuja, K. Chaudhari, G. Paramasivam, G. Ragupathy, J. S. Mohanty, T. Pradeep, J. Phys. Chem. C 2021, 125, 3553–3566.

[26] Z. Wang, L. J. Rothberg, J. Phys. Chem. B 2005, 109, 3387–3391.

[27] Y. Maruyama, M. Ishikawa, M. Futamata, J. Phys. Chem. B 2004, 108, 673–678.

[28] A. Kudelski, Chem. Phys. Lett. 2006, 427, 206–209.

[29] G. Smith, J. S. Girardon, J. F. Paul, E. Berrier, Phys. Chem. Chem. Phys. 2016, 18, 19567–19573.

[30] A. R. Prado, D. O. de Souza, J. P. Oliveira, R. H. A. Pereira, M. C. C. Guimarães, B. v. Nogueira, P. v. Dixini, M. R. N. Ribeiro, M. J. Pontes, Appl. Spectrosc. 2017, 71, 2670–2680.

[31] D. B. Grys, B. de Nijs, A. R. Salmon, J. Huang, W. Wang, W. H. Chen, O. A. Scherman, J. J. Baumberg, ACS Nano 2020, 14, 8689–8696.

[32] J.-W. Park, J. S. Shumaker-Parry, J. Am. Chem. Soc. 2014, 136, 1907–1921.

[33] M. Mabuchi, T. Takenaka, Y. Fujiyoshi, N. Uyeda, Surf. Sci. 1982, 119, 150–158.

[34] C. H. Munro, W. E. Smith, M. Garner, J. Clarkson, P. C. White, Langmuir 1995, 11, 3712–3720.

[35] O. Siiman, L. A. Bumm, R. Callaghan, C. G. Blatchford, M. Kerker, J. Phys. Chem. 1983, 87, 1014–1023.

[36] D. Grasseschi, R. A. Ando, H. E. Toma, V. M. Zamarion, RSC Adv. 2015, 5, 5716–5724.

[37] A. Ferrari, J. Robertson, Phys. Rev. B 2000, 61, 14095.

[38] N. P. W. Pieczonka, R. F. Aroca, ChemPhysChem 2005, 6, 2473–2484.

[39] I. Noda, Y. Ozaki, Two-Dimensional Correlation Spectroscopy – Applications in Vibrational and Optical Spectroscopy, John Wiley & Sons, Ltd, Chichester, 2004.

[40] K. J. Maynard, M. Moskovits, J. Chem. Phys. 1998, 90, 6668.

[41] S. A. Hunter-Saphir, J. A. Creighton, J. Raman Spectrosc. 1998, 29, 417–419.

[42] P. A. Giguére, T. K. K. Srinivasan, J. Raman Spectrosc. 1974, 2, 125–132.

[43] H. Nakatsuji, Z. M. Hu, H. Nakai, K. Ikeda, Surf. Sci. 1997, 387, 328–341.

[44] N. Ohta, K. Nomura, I. Yagi, J. Phys. Chem. C 2012, 116, 14390–14400.

[45] J. Kim, A. A. Gewirth, J. Phys. Chem. B 2006, 110, 2565–2571.

[46] C. Li, H. Xiong, M. He, B. Xu, Q. Lu, ACS Catal. 2021, 11, 12029–12037.

[47] A. Kudelski, B. Pettinger, Chem. Phys. Lett. 2000, 321, 356–362.

[48] B. N. Pramanik, A. K. Ganguly, M. L. Gross, Applied Electrospray Mass Spectrometry, Marcel Dekker, New York, 2002.

[49] T. Kind, O. Fiehn, Bioanal. Rev. 2010, 2, 23–60.

[50] M. Holčapek, R. Jirásko, M. Lísa, J. Chromatogr. A 2010, 1217, 3908–3921.

[51] G. E. Johnson, J. Laskin, Analyst 2016, 141, 3573–3589.

[52] J. B. Tracy, M. C. Crowe, J. F. Parker, O. Hampe, C. A. Fields-Zinna, A. Dass, R. W. Murray, J. Am. Chem. Soc. 2007, 129, 16209–16215.

[53] M. Wuithschick, A. Birnbaum, S. Witte, M. Sztucki, U. Vainio, N. Pinna, K. Rademann, F. Emmerling, R. Kraehnert, J. Polte, ACS Nano 2015, 9,7052–7071.

[54] M. v. Gorbachevskii, D. S. Kopitsyn, M. S. Kotelev, E. v. Ivanov, V. A. Vinokurov, A. A. Novikov, RSC Adv. 2018, 8, 19051–19057.

[55] M. Moskovits, J. S. Suh, J. Am. Chem. Soc. 1985, 107, 6826–6829.

[56] V. H. S. de Melo, V. M. Zamarion, K. Araki, H. E. Toma, J. Raman Spectrosc. 2011, 42, 644–652.

[57] M. M. Barbooti, D. A. Al-Sammerrai, Thermochim. Acta 1986, 98, 119–126.

[58] D. Wyrzykowski, E. Hebanowska, G. Nowak-Wiczk, M. Makowski, L. Chmurzyński, J. Therm. Anal. Calorim. 2011, 104, 731–735.